Stochastic model for quantifying effect of surface roughness on light reflection by diffuse reflectance standards

Peng Tian,[a,b,c] Xun Chen,[d] Jiahong Jin,[a,b,c] Jun Q. Lu,[a,b] Xiaohui Liang,[e] and Xin-Hua Hu[a,b,*]
[a]Institute for Advanced Optics, Hunan Institute of Science and Technology, Yueyang, China
[b]East Carolina University, Department of Physics, Greenville, North Carolina, United States
[c]Hunan Institute of Science and Technology, School of Physics and Electronics Science, Yueyang, China
[d]Clemson University, Department of Bioengineering and COMSET, CU-MUSC Bioengineering Program, Charleston, South Carolina, United States
[e]AMMS, Experimental Instrument Plant, Beijing, China

1

Abstract. Diffuse reflectance standards of known hemispherical reflectance R_h are widely used in optical and imaging studies. We have developed a stochastic surface model to investigate light reflection and roughness dependence. Through Monte Carlo simulations, the angle-resolved distributions of reflected light have been modeled as the result of local surface reflection with a constant reflectance R_s representing the overall ability of a reflectance standard. The surface was modeled by an ensemble of random Gaussian surface profiles parameterized by a mean surface height δ and transverse correlation length a. By decreasing δ/a, the calculated reflected light distributions were found to transit from Lambertian to specular reflection regime. Reflected light distributions were measured with three standards with nominal reflectance R_h valued at 10%, 80%, and 99%. The calculated results agree well with the measured data in their angular distributions at different incident angles by setting $R_s = R_h$ and $\delta = a = 3.5\ \mu$m. © *2018 Society of Photo-Optical Instrumentation Engineers (SPIE)* [DOI: 10.1117/1.OE.57.XX.XXXXXX]

Keywords: reflectance standard; scattering; rough surface; Monte Carlo simulation.

Paper 181041 received Jul. 18, 2018; accepted for publication Aug. 28, 2018.

1 Introduction

Diffuse reflectance standards are very useful devices for calibrating instrument and sensors designed for light reflection measurement in, for example, multispectral reflectance analysis of materials and remote sensing.[1–6] The rough surfaces of these devices are critical for hemispherical dispersion of reflected light intensity. A key challenge is to understand quantitatively the dependence of reflected light distribution on the degree of surface roughness. Extensive literature is available on device construction, spectral calibration, and angular characterization of the reflected light distribution.[7–12] In contrast, much remains to be learned about the effect of surface roughness and its modeling.[13,14] Clear understanding of relations between surface roughness and light distribution by diffuse reflectance standards is significant for not only essential insight on but also accurate simulation of objects in machine vision that carry ubiquitously rough surfaces.[9,15–19] In this report, we present a stochastic rough surface model of diffuse reflectance implemented by Monte Carlo (MC) simulations to analyze directional-hemispherical light reflection. The model employs an effective surface treatment of turbid samples that is simplified from our previous models of biological tissues with rough surfaces to allow detailed study of surface-roughness dependence of light reflection with significantly reduced simulation times.[20–23] The calculated angular distributions of reflected light are compared to the measured data obtained with diffuse reflectance standards of known hemispherical reflectance values. Besides its theoretical implications, the ability to understand and simulate the angular distribution of the hemispherically reflected light provides a quantitative and touch-free means to reveal surface roughness of diffuse reflectance standards and other devices producing diffuse reflection.

2 Methods

2.1 *Diffuse Reflectance Standards and Light Measurement*

Diffuse reflectance standards are made of sintered polytetrafluoroethylene (PTFE) resin in powder form.[7,24] With a rough surface and porous structure, the PTFE layer of a few millimeters in thickness acts as strong turbid target, which scatters incident light into the hemispherical space diffusely.[7] By doping with black pigments, the nominal values of hemispherical reflectance R_h can be adjusted and remain as a constant approximately in a wide spectral region from 350 to 1800 nm. To validate the effective surface model for this study, we have performed angle-resolved measurement of light reflected from each of three standards illuminated by a monochromatic beam of wavelength λ and incident angles (θ_{i0}, ϕ_{i0}). A photodiode (FDS100, Thorlabs) rotating on a semicircular orbit of radius r_d was used to detect reflected light intensity $I_R(\theta_r, \phi_r)$ in the y-z plane with $\varphi_r = 90$ deg or -90 deg. Both sets of angles, (θ_{i0}, ϕ_{i0}) and (θ_r, ϕ_r), are defined by the Cartesian coordinate system shown in Fig. 1(a) that also illustrates the experimental configuration of reflection measurement.

*Address all Correspondence to: Xin-Hua Hu, E-mail: hux@ecu.edu

0091-3286/2018/$25.00 © 2018 SPIE

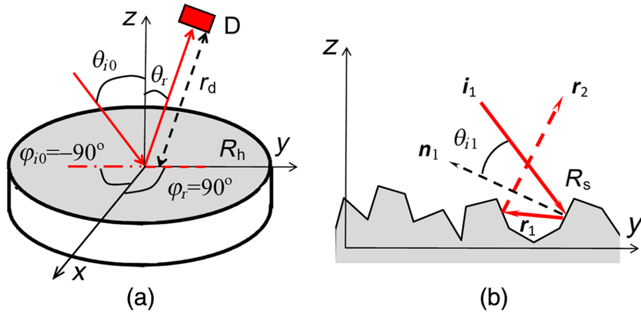

Fig. 1 (a) Schematic of reflection measurement with (θ_{i0}, ϕ_{i0}) for incident beam direction and a detector D located at r_d for detecting $I_R(\theta_r, \phi_r)$; (b) simulation configuration of light reflected at $\mathbf{r} = (\boldsymbol{\rho}, z)$ with $\mathbf{i}_m$ ($m = 1$) as unit vector of incident direction, θ_{im} as local incident angle, $\mathbf{r}_m$ and $\mathbf{r}_{m+1}$ as of reflection directions and R_s as local surface specular reflectance. The surface profile in (b) is shifted upward for clear presentation.

2.2 *Modeling of Light Reflection by a Diffuse Reflectance Standard*

Turbid materials like PTFE layers with rough surfaces can be modeled conventionally according to the radiative transfer theory for treatment of absorption and scattering in the bulk and the Fresnel equations for accounting of specular reflections at the surface. The computational cost of such an implementation, however, is very high using the statistical approach of MC simulations.[21–23] In addition, the hemispherical reflectance R_h determined for each diffuse reflectance standard provides the ratio of integrated reflected light to the incident light. As a result, we intend to develop an effective surface model that is capable of characterizing surface roughness of turbid objects with known R_h without the time-consuming photon-tracking in the bulk as shown in our previous studies.[21–23] A local surface reflectance R_s is defined for this purpose to quantify the ability of a turbid object, such as a PTFE layer for light reflection at surface and by bulk scattering. Furthermore, local surface reflections are treated as specular ones by a randomly rough surface across the x-y transverse plane at $z = 0$. The surface profile is described by $z = \zeta(\boldsymbol{\rho})$, where z represents the surface height at a transverse location given by $\rho = (x, y)$ based on a previous model of light interaction with rough surface.[21] The simulation method is briefly summarized below in the context of diffuse reflectance standards.

Since the wavelength of incident light is much smaller than the transverse dimensions of examined area on the surface of a reflectance standard, one can replace the electromagnetic field of the incident beam at $\mathbf{r} = (\rho, z)$ of a rough surface by a field existing on the plane tangential to the surface at $\mathbf{r}$.[20] This plane approximation allows us to model the rough surface of a diffuse reflectance standard as a mesh of triangular elements with a local reflectance R_s. As stated above, we further assume that the local surface reflection is specular in nature with R_s, representing the overall ability to reflect light by the standard in order to significantly reduce computational time. For comparison to the measured data, the value of R_s is related to the calibrated reflectance value R_h of the diffuse reflectance standard provided by the vendor. Under these assumptions, reflection of incident light by a standard depends on the surface profile in terms of local incidence angle and R_s characterizing the light–matter interaction for the reflectance standard.

A rough surface of profile given by $z = \zeta(\rho)$ is numerically generated as a stationary stochastic process characterized by a Gaussian function of correlation between two locations of $\boldsymbol{\rho}$ and $\boldsymbol{\rho}'$ and a zero mean. The random numbers used for z must satisfy

$$\langle \zeta(\boldsymbol{\rho})\zeta(\boldsymbol{\rho}')\rangle = \delta^2 \exp[-(\boldsymbol{\rho} - \boldsymbol{\rho}')^2/a^2] \tag{1}$$

and

$$\langle \zeta(\boldsymbol{\rho})\rangle = 0, \tag{2}$$

where δ is the rms value of the surface departure from the mean surface of $x - y$ plane describing the height fluctuation and a is the transverse correlation length of the surface roughness. An MC code has been developed to calculate reflected light distribution $I_{Rc}(\theta_r, \varphi_r)$ that can be compared to the measured data of $I_R(\theta_r, \phi_r)$. To fulfill the stochastic requirement, MC simulations of light reflection by the rough surface characterized with a parameter set of (a, δ) have been performed on an ensemble of 50 statistically independent surface profiles $z = \zeta(\rho)$ satisfying both Eqs. (1) and (2). The reflected light distributions calculated from the 50 profiles were summed to obtain ensemble averaged $I_{Rc}(\theta_r, \phi_r)$, as indicated by the angular brackets in Eqs. (1) and (2).

All rough surface profiles were set to the same square areas of 1 mm side length to reduce memory requirement and are divided into a grid of 501×501 basic units on the x–y plane with grid points $\boldsymbol{\rho}_{ij}$ and $-250 \le i, j \le 250$. The incident beam is represented by N_0 photons injected over the area of a profile scaled down from the measured beam profile on x–y plane. The transverse locations $\boldsymbol{\rho}$ of injected photons are determined by two random numbers that were transformed from uniform distributions between 0 and 1 into numerical distributions along x- and y-axis that are consistent with the measured profile of the incident beam. Each photon injected on a surface profile hits the surface M times before it exits. The maximum value of M was truncated to 20 to avoid long loops of tracking in the MC simulations with negligible loss of accuracy. At each hitting location, a random number RN uniformly distributed between 0 and 1 is compared to the predetermined surface specular reflectance R_s. The tracked photon is reflected if $\mathrm{RN} \le R_s$ or absorbed if $\mathrm{RN} > R_s$. A reflected photon is propagated along the specular reflection direction determined by a triangle mesh representing one of the 50 profiles.

As detailed in Ref. 21, rough surface heights $z_{ij} = \zeta(\boldsymbol{\rho}_{ij})$ at grid points $\boldsymbol{\rho}_{ij}$ are generated randomly for MC simulations with distributions satisfying Eqs. (1) and (2). Thus, each rough surface profile, as viewed in Fig. 1(b), is made of a mesh of triangular elements that can be projected to the $x - y$ plane as one pair of triangles dividing equally a square grid unit, as shown in Fig. 2(a), by the blue and red colored zones. The mesh elements also serve as the tangential planes to the photon hitting location $\mathbf{r} = (\rho, z)$ employed by the plane approximation discussed above. Figure 2(b) presents the projection of an element pair of the surface mesh to the x–y plane surrounded by eight nearest-neighbor element pairs with projections shown in faded colors. A photon hitting a surface element can be reflected to hit the other element supported by the same grid unit or one of the 16 elements in the nearest-neighbor element pairs. To reduce the

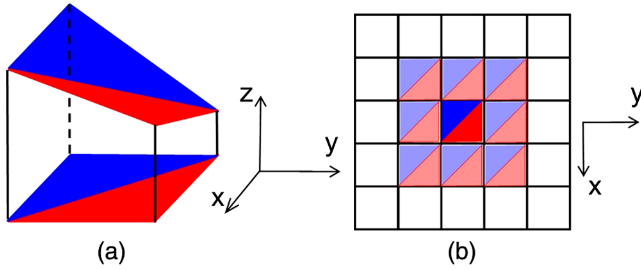

Fig. 2 Schematic representation of (a) a pair of triangular elements of a rough surface profile mesh projected to a square grid unit of the $x-y$ plane and (b) an element pair projected to a grid unit of the $x-y$ plane ($z=0$) in bright colors and other eight nearest-neighbor element pairs projected in faded colors.

complexity of modeling, we neglect secondary hits of surface elements beyond the nearest-neighbor pairs, which were verified to affect little the calculated results. By applying restrictions on z coordinates of hitting locations and directional cosine along the z-axis, the number of possible triangular elements hit by a reflected photon can be reduced to nine or less on average to reduce simulation time.

Once a photon hits a mesh element at $\mathbf{r}$, the local surface normal vector $\mathbf{n}_m$ is first calculated by

$$\mathbf{n}_m = \frac{-\zeta_x'\mathbf{x} - \zeta_y'\mathbf{y} + \mathbf{z}}{\sqrt{\zeta_x'^2 + \zeta_y'^2 + 1}}, \tag{3}$$

where $m = 1, \ldots, M$ is the sequence number of reflection, $\mathbf{x}, \mathbf{y}$, and $\mathbf{z}$ are the basis vectors, ζ_x' and ζ_y' are partial derivatives of surface profile function $\zeta(\rho)$. From Eq. (3), one can derive the incident angle θ_{im} given the unit vectors of $\mathbf{i}_{\mathrm{m}}$ for the incident direction of a tracked photon and $\mathbf{r}_{\mathbf{m}}$ for specular reflection direction. The interception of a reflected photon along $\mathbf{r}_{\mathrm{m}}$ with a neighboring element is determined using algorithms widely used in computational geometry.[25] Photon reflection and tracking among surface elements continue with $(\mathbf{i}_{\mathrm{m}}, \mathbf{r}_{\mathrm{m}})$ updated until it exits from the surface from the last reflection site at $\mathbf{r}_{\mathrm{m}}$. A total of 17 detection bins were used in the MC code to obtain $I_{\mathrm{Rc}}(\theta_{\mathrm{r}}, \varphi_{\mathrm{r}})$ or $I_{\mathrm{Rc}}(\eta)$, which are arranged on a semicircular orbit of r_{d} from the center of rough surface according to the experimental system. The bins are marked with a rotation angle η defined by $\theta_{\mathrm{r}}\,\sin\varphi_{\mathrm{r}}$ of the photons exiting from a rough surface. For comparison to the measured data of I_{R}, the center angular position η of the bins ranges from -40 deg to 40 deg in steps of 5 deg. The detection bins have identical areas scaled down from that of the photodiode sensor by the same factor sued for scaling the illuminated area in MC simulations from the measured one.

3 Results

Three diffuse reflectance standards were used in this study that are of 50.8 mm in diameter and $R_{\mathrm{h}} = 99\%$, 80%, and 10% in nominal reflectance (SRS-99-020, SRS-80-020, SRS-10-020, Labsphere Inc.). Distribution of light reflected from a standard was measured as $I_{\mathrm{R}}(\theta_{\mathrm{r}}, \varphi_{\mathrm{r}})$ with a photodiode of $3.6 \times 3.6\ \mathrm{mm}^2$ in area and rotating on a circular orbit of $r_{\mathrm{d}} = 70$ mm, as shown in Fig. 1(a). A monochromatic incident beam of λ in wavelength was obtained from a xenon light source and a monochromator. The

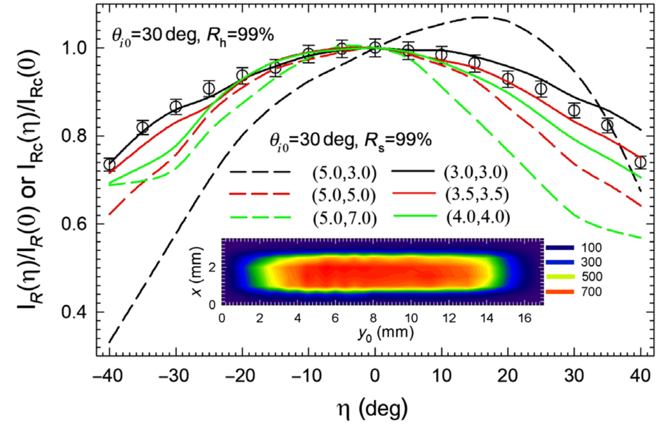

Fig. 3 Normalized intensity of reflected light versus rotation angle $\eta = \theta_{\mathrm{r}} \sin \phi_{\mathrm{r}}$ with symbols and error bars for $I_{\mathrm{R}}(\eta)$ measured at $\lambda = 880$ nm from a diffuse reflectance standard of $R_{\mathrm{h}} = 99\%$ and solid lines for $I_{\mathrm{Rc}}(\eta)$ calculated with $R_{\mathrm{s}} = 99\%$ and ensembles rough surfaces generated using different combinations of (a, δ) in μm. Inset: incident beam profile measured in the transverse x-y_0 plane with color bars representing photodiode signals in μV.

beam was collimated by spherical mirrors with a divergence angle of about 2.5 deg before incidence on a standard. Measurements of angle-resolved distributions of reflected light have been performed with $\lambda = 880$ nm for the center wavelength and 3 nm in bandwidth. The incident beam profile was measured in the plane transverse to the incident direction and displayed as the inset of Fig. 3. The profile was found to be rectangular with half-maximum sizes of about $2.0\ \mathrm{mm} \times 13$ mm along, respectively, the x- and y_0-axis in the transverse plane. The measured profile of incident beam has been used to obtain a numerically normalized distribution for injection of N_0 photons in each of the MC simulations performed on a rough surface profile described in Eq. (1).

The center directions of incident beam and reflected light acquired by the photodiode are given by $(\theta_{i0}, \varphi_{i0})$ and $(\theta_{\mathrm{r}}, \varphi_{\mathrm{r}})$, respectively, with $\varphi_{i0} = -90$ deg and $\varphi_r = 90$ deg or -90 deg. To increase signal-to-noise ratio, the incident beam was modulated by a mechanical chopper at $f_0 = 20$ Hz and the acquired photodiode signals were amplified and digitized by a 16-bit A/D convertor. Fourier transform was performed to extract the signal component at f_0 for $I_{\mathrm{R}}(\eta)$. For each standard, we performed three measurements of I_{R} for calculation of mean values and standard deviations. Figure 3 presents the normalized intensity of $I_{\mathrm{R}}(\eta)$ measured with the standard of $R_{\mathrm{h}} = 99\%$ by symbols and error bars and examples of normalized calculated curves of $I_{\mathrm{Rc}}(\eta)$ with $R_{\mathrm{s}} = R_{\mathrm{h}}$ and different combinations of a and δ for $\theta_{i0} = 30$ deg and $\varphi_{i0} = -90$ deg. The examples of the calculated curves $I_{\mathrm{Rc}}(\eta)$ are in two groups: one with $a = 5.0\ \mu$m by dash lines and one with $a = \delta$ by solid lines. One can observe from the group of dash lines that $I_{\mathrm{Rc}}(\eta)$ appears symmetric when δ/a is close to 1 and showing a peak toward the specular reflection direction of a flat surface when δ/a decreases from 1. These results demonstrate that the stochastic surface model presented in this report can yield reflection regimes from Lambertian for significantly rough surfaces to specular for smoother surfaces by varying δ/a with a constant R_s. For $a = \delta$, the $I_{\mathrm{Rc}}(\eta)$ curves in the solid-line group exhibit symmetric and approximate Lambertian shapes,

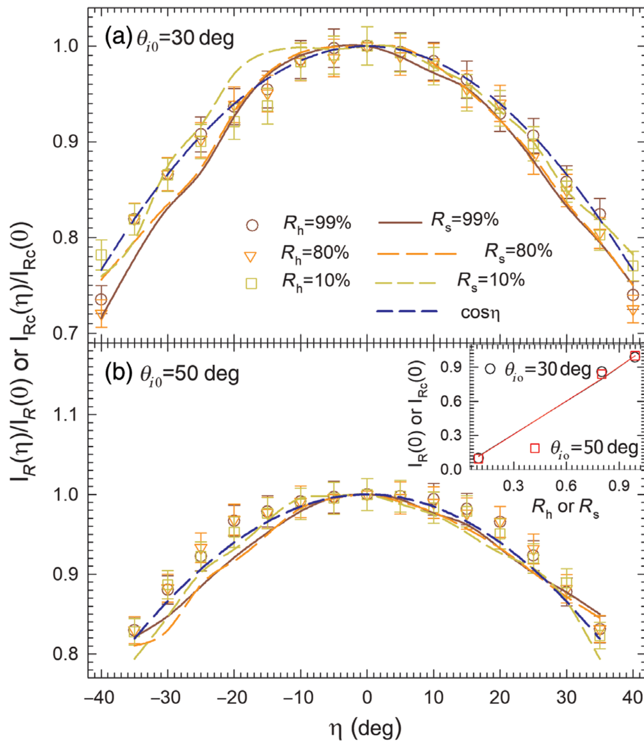

Fig. 4 Normalized intensity of reflected light versus rotation angle η with symbols and error bars for $I_R(\eta)$ measured at $\lambda = 880$ nm from three diffuse reflectance standards and solid lines for $I_{Rc}(\eta)$ calculated with $a = \delta = 3.5$ μm and incident angle of (a) $\theta_{i0} = 30$ deg; (b) $\theta_{i0} = 50$ deg. Inset: $I_{Rc}(0)$ versus R_h (symbols) and $I_{Rc}(0)$ versus R_s (lines). The angular dependence of Lambertian reflectance is represented by blue dash lines.

which is comparable to the measured data of $I_R(\eta)$. Hence, we varied values of a under the condition of $a = \delta$ to fit $I_{Rc}(\eta)$ to $I_R(\eta)$, as shown in Fig. 3, by the solid lines. Good agreements between $I_{Rc}(\eta)$ to $I_R(\eta)$ can be achieved when a was set to between 3.0 and 3.5 μm.

Measurements and MC simulations of reflected light distribution have been carried out with two more diffuse reflectance standards of $R_h = 80\%$ and 10% at multiple incident angles of θ_{i0}. Figure 4 plots the normalized data of $I_R(\eta)$ acquired from the three standards at two values of θ_{i0} for comparison and only the normalized calculated curves of $I_{Rc}(\eta)/I_{Rc}(0)$ with $R_s = R_h$ and surface parameters set to $a = \delta = 3.5$ μm. Again, the calculated curves fit well to the measured data on their angular dependences, as shown in Figs. 4(a) and 4(b), and the dependences of intensity at $\eta = 0$ on R_s or R_h, as shown in the inset. Larger fluctuations can be observed in $I_{Rc}(\eta)$ calculated with $R_s = 10\%$, since incident photons have much higher probability to be absorbed or terminated before exit the surface and hit one of detection bins.

4 Discussion

The diffuse reflectance standards considered here can be regarded as turbid media for their porous structures in the sense of irregular orientations of surface elements and granular constituents of bulk leading to heterogeneity in refractive index distribution. Without doping, the pressed PTFE powders exhibit little absorption and strong scattering due to the large refractive index mismatch between PTFE (~1.35 in visible and near-infrared regions)[26] and air. As a result, the steady-state distribution of light reflected from such an object is a consequence of specular reflection at surface and multiple scattering in bulk. Various analytical and numerical methods have been developed to consider such cases of light–matter interaction as random media consisting simple shaped inclusions and/or 1-D randomly rough surfaces by effective medium theories or extended variants.[27,28] These existing methods of field theory, however, are very difficult to be applied here due to complex and unknown details on surface profile and bulk composition. The multiple scattering in turbid materials can also be modeled using the radiative transfer theory and implemented in MC simulation for treatment of rough surfaces.[21–23] While feasible, such endeavors often require multiple optical parameters, such as absorption and scattering coefficients that are wavelength dependent and unavailable for many types of turbid samples. In addition, high cost of code development and computational resources is needed to perform such numerical studies.

In this study, we developed a different and simplified surface model to examine the effect of surface roughness on the reflected light distributions by diffuse reflectance standards with known hemispherical reflectance R_h. By using a local surface reflectance R_s representing the overall ability of light reflection, the simplified model allows rapid calculation of reflected light distribution of a standard, which is represented as a rough surface profiled as a mesh of stochastically implemented triangular elements, as illustrated in Fig. 2. As shown in Figs. 3 and 4, the calculated results of reflected light distribution agree well with the measured data of three diffuse reflectance standards if R_s is set as a constant and $R_s = R_h$. The modeling of rough surface of a standard as stochastic mesh of local flats is consistent with the tangential plane approximation of the field theory that requires local surface sizes to be much larger than the light wavelength λ,[20] which is satisfied by the sizes of the surface profile parameters a and δ around 3 μm derived by curve fitting.

By assuming R_s as a constant, the calculated light reflection can approach approximate Lambertian regime only for the cases of $a \sim \delta$. We note from Eq. (1) that a and δ represent statistically and, respectively, the characteristic lengths of transverse locations and vertical variations of, for example, peak-to-peak changes in a surface profile $\zeta(\rho)$. Consequently, a/δ can be regarded as the average slope angle of the profile and $a \sim \delta$ indicates the condition of slope angle around 45 deg for the ensemble of surface profiles. This outcome suggests that objects exhibiting diffuse reflection appearances that are of approximate Lambertian type should likely possess the same surface profile feature of $a \sim \delta$, as revealed in this report. It is also interesting to note from the calculated curves of I_{Rc} in Fig. 3 that under the condition of $a = \delta$, increasing the value of a or the size of surface roughness leads to steeper decrease of light intensity as η moves away from 0. These results could be used to quantify surface roughness indirectly by straightforward measurement of $I_R(\eta)$ in the cases of diffuse reflectance standards or samples with Lambertian or similar types of diffuse reflection.

Acknowledgments

P.T. acknowledges a visiting scholarship from China Scholarship Council (Grant No. 201508430225) and a

research grant from the Education Department of Hunan Province, China (Grant No. 14A062). The authors thank Mr. Jue Ding for performing a part of data acquisition.

References

1. R. L. P. Van Veen, W. Verkruysse, and H. Sterenborg, "Diffuse-reflectance spectroscopy from 500 to 1060 nm by correction for inhomogeneously distributed absorbers," *Opt. Lett.* **27**(4), 246–248 (2002).
2. U. Utzinger and R. R. Richards-Kortum, "Fiber optic probes for biomedical optical spectroscopy," *J. Biomed. Opt.* **8**(1), 121–147 (2003).
3. R. A. Viscarra Rossel et al., "Visible, near infrared, mid infrared or combined diffuse reflectance spectroscopy for simultaneous assessment of various soil properties," *Geoderma* **131**(1), 59–75 (2006).
4. G. T. Georgiev and J. J. Butler, "Long-term calibration monitoring of Spectralon diffusers BRDF in the air-ultraviolet," *Appl. Opt.* **46**(32), 7892–7899 (2007).
5. G. N. Stamatas et al., "In vivo measurement of skin erythema and pigmentation: new means of implementation of diffuse reflectance spectroscopy with a commercial instrument," *Br. J. Dermatol.* **159**(3), 683–690 (2008).
6. P. Tian et al., "Quantitative characterization of turbidity by radiative transfer based reflectance imaging," *Biomed. Opt. Express* **9**(5), 2081–2094 (2018).
7. V. R. Weidner and J. J. Hsia, "Reflection properties of pressed polytetrafluoroethylene powder," *J. Opt. Soc. Am.* **71**(7), 856–861 (1981).
8. M. D. Fairchild and D. J. O. Daoust, "Goniospectrophotometric analysis of pressed PTFE powder for use as a primary transfer standard," *Appl. Opt.* **27**(16), 3392–3396 (1988).
9. G. J. Ward, "Measuring and modeling anisotropic reflection," *ACM SIGGRAPH Comput. Graphics* **26**(2), 265–272 (1992).
10. A. Ferrero et al., "Spectral and geometrical variation of the bidirectional reflectance distribution function of diffuse reflectance standards," *Appl. Opt.* **51**(36), 8535–8540 (2012).
11. J. M. Sanz, C. Extremiana, and J. M. Saiz, "Comprehensive polarimetric analysis of Spectralon white reflectance standard in a wide visible range," *Appl. Opt.* **52**(24), 6051–6062 (2013).
12. T. A. Germer, "Full four-dimensional and reciprocal Mueller matrix bidirectional reflectance distribution function of sintered polytetrafluoroethylene," *Appl. Opt.* **56**(33), 9333–9340 (2017).
13. H. E. Bennett and J. O. Porteus, "Relation between surface roughness and specular reflectance at normal incidence," *J. Opt. Soc. Am.* **51**(2), 123–129 (1961).
14. B. van Ginneken, M. Stavridi, and J. J. Koenderink, "Diffuse and specular reflectance from rough surfaces," *Appl. Opt.* **37**(1), 130–139 (1998).
15. R. L. Cook and K. E. Torrance, "A reflectance model for computer graphics," *ACM Trans. Graphics* **1**(1), 7–24 (1982).
16. X. D. He et al., "A comprehensive physical model for light reflection," *ACM SIGGRAPH Comput. Graphics* **25**(4), 175–186 (1991).
17. K. J. Dana et al., "Reflectance and texture of real-world surfaces," *ACM Trans. Graphics* **18**(1), 1–34 (1999).
18. S. P. Mallick et al., "Beyond Lambert: reconstructing specular surfaces using color," in *IEEE Computer Society Conf. on Computer Vision and Pattern Recognition (CVPR'05)*, Vol. **612**, pp. 619–626 (2005).
19. H. Andreas and H. Kai-Olaf, "Three-dimensional appearance characterization of diffuse standard reflection materials," *Metrologia* **47**(3), 295–304 (2010).
20. P. Beckman and A. Spizzichino, *The Scattering of Electromagnetic Waves from Rough Surfaces*, Pergamon, London (1963).
21. J. Q. Lu, X. H. Hu, and K. Dong, "Modeling of the rough-interface effect on a converging light beam propagating in a skin tissue phantom," *Appl. Opt.* **39**(31), 5890–5897 (2000).
22. X. Ma, J. Q. Lu, and X. H. Hu, "Effect of surface roughness on determination of bulk tissue optical parameters," *Opt. Lett.* **28**(22), 2204–2206 (2003).
23. X. Ma et al., "Bulk optical parameters of porcine skin dermis tissues at eight wavelengths from 325 to 1557 nm," *Opt. Lett.* **30**(4), 412–414 (2005).
24. C. J. Bruegge et al., "Use of spectralon as a diffuse reflectance standard for in-flight calibration of earth-orbiting sensors," *Opt. Eng.* **32**(4), 805–814 (1993).
25. J. O'Rourke, *Computational Geometry in C*, Cambridge University Press, Cambridge, New York (1998).
26. K.-I. Tsunoda et al., "The use of poly(tetrafluoroethylene-co-hexafluoropropylene) tubing as a waveguide capillary cell for liquid absorption spectrometry," *Appl. Spectrosc.* **44**(1), 163–165 (1990).
27. R. G. Barrera and A. Garcia-Valenzuela, "Coherent reflectance in a system of random Mie scatterers and its relation to the effective-medium approach," *J. Opt. Soc. Am. A* **20**(2), 296–311 (2003).
28. H. C. van de Hulst, "*Multiple Light Scattering: Tables, Formulas, and Applications*," Academic Press, New York (1980).

Peng Tian received his MS and PhD degrees in optical engineering from Huazhong University of Science and Technology in China and his major research interests are on the optical properties of biological tissues and turbid materials.

Xun Chen has an MS degree in biomedical engineering received from Tianjin University in China and is currently a PhD student in the study of fluorescence imaging of biological cells.

Jiahong Jin received his MS degree in optics from Sun Yat-Sen University in China and is pursuing a PhD degree in biomedical engineering in the direction of multispectral imaging of biological tissues.

Jun Q. Lu received her MS degree from Nankai University in China and PhD degree from the University of California at Irvine, both in physics. Her main interests of research are in the theoretical and numerical modeling of light-tissue and light–cell interactions.

Xiaohui Liang received her MS degree in biomedical engineering from Tianjin University in China and her research interests are in the field of precision instrumentation.

Xin-Hua Hu received his MS degree in physics from Nankai University in China and Indiana University at Bloomington and PhD degree in physics from University of California at Irvine. His research interests are on light interaction with biological tissues and cells.